Electronic structure of the Si(110)-(16×2) surface: High-resolution ARPES and STM investigation

Kazuyuki Sakamoto,[1,*] Martin Setvin,[2,†] Kenji Mawatari,[3] P. E. J. Eriksson,[4] Kazushi Miki,[2] and R. I. G. Uhrberg[4]
[1]*Graduate School of Advanced Integration Science, Chiba University, Chiba 263-8522, Japan*
[2]*National Institute for Materials Science, Ibaraki 305-0044, Japan*
[3]*Department of Physics, Graduate School of Science, Tohoku University, Sendai 980-8578, Japan*
[4]*Department of Physics, Chemistry, and Biology, Linköping University, S-581 83 Linköping, Sweden*
(Received 9 October 2008; revised manuscript received 28 November 2008; published 8 January 2009)

The electronic structure of a single domain Si(110)-(16×2) surface has been investigated by high-resolution angle-resolved photoelectron spectroscopy and scanning tunneling microscopy (STM). Four semiconducting surface states with flat dispersions, whose binding energies are 0.2, 0.4, 0.75, and 1.0 eV, were observed in the bulk band gap and more than six states were observed within the projected bulk band at binding energies less than 5.2 eV. The origins of the four surface states and of one state at a binding energy of approximately 1.5 eV at the $\bar{\Gamma}$ point are discussed based on the local density of states mappings obtained by STM. Further, a structural model that can explain all these five states is proposed.

DOI: 10.1103/PhysRevB.79.045304 PACS number(s): 73.20.At, 79.60.−i, 68.35.bg, 68.37.Ef

I. INTRODUCTION

Of the low index planes of Si, Si(110) is a surface that has an anisotropic structure. A surface with an anisotropic structure is a good template to grow nanowires, and in fact Si(110) has been used to grow nanowires such as dysprosium silicide nanowires,[1] iron silicide nanowires,[2] Pb nanowires,[3] Au atomic wires,[4] and Sn wires.[5] Further, due to the slightly higher surface energy of Si(110) ($\gamma_{(110)} > \gamma_{(001)} > \gamma_{(111)}$),[6,7] Si nanowires are reported to grow along the [110] direction with a hexagonal cross section of the (110) face, bounded by two {001}-type facets and four $\{\bar{1}11\}$-type facets.[7–11] Together with the importance to make nanowires, the Si(110) surface has also a technological importance for fabricating complementary metal-oxide semiconductor (CMOS) circuits with high hole mobility. The CMOS transistor based on a Si(110) surface is reported to have a higher hole mobility than one based on a Si(001) surface.[12,13] However, despite of such increasing interest, the physical properties of the Si(110) clean surface are still not well understood.

The clean Si(110) surface exhibits a reconstruction that is commonly denoted as (16×2) (Refs. 14–20) since 16× superstructure spots are observed between the fundamental (00) and $(\bar{1}1)$ spots in electron diffraction.[14–16] A large number of studies has been performed to determine the atomic structure of Si(110)-(16×2), and several models have been proposed to explain both the up and down regular step arrangements and the pentamers observed using scanning tunneling microscopy (STM).[16–21] Of the proposed models, the surface energy of the adatom-tetramer-interstitial (ATI) structure has been reported to be slightly lower than those of the other models.[22,23] Taking the simulated STM images into account, the pentamer observed in STM is concluded to be formed by four adatoms (a tetramer) and one first layer Si atom in the ATI model.

Compared to the large number of studies on the atomic structure, only a few studies have been performed on the valence electronic structure of Si(110)-(16×2). The early studies[24,25] have reported the presence of four surface states at binding energies (E_B) less than 5 eV, and a 0.6 eV dispersion width of the surface state with the smallest E_B.[24] In contrast to these results, a recent photoemission study reports the presence of two surface states in the bulk band gap.[26] The E_B of these states are 0.4 and 0.9 eV and their dispersion widths are below 0.2 eV. Together with these two surface states, three states that hardly disperse have been observed within the projected bulk band. However, the origins of these three states are not discussed and thus the number of surface states is still not determined. Since a proper understanding on the valence electronic structure is essential to comprehend the physical properties of the Si(110)-(16×2) surface, a surface sensitive high-resolution angle-resolved photoelectron spectroscopy (ARPES) measurement and a local density of states (LDOS) mapping using STM are required.

In this paper, we present detailed ARPES measurements performed along the $[00\bar{1}]$, $[\bar{1}10]$, and $[\bar{1}1\bar{1}]$ directions of the Si(110)-(16×2) surface and the LDOS mapping of the surface obtained using STM. Four flat surface state bands, none of which crosses the Fermi level, were observed in the bulk band gap. The number of surface states observed in the band gap is larger than those reported in the literature. The origins of these four states are discussed based on their E_B, the LDOS mappings, and the proposed structural model. We also discuss the dispersion behaviors of the six states observed within the projected bulk band and the origin of one of them.

II. EXPERIMENTAL DETAILS

The high-resolution photoemission (PES) measurements were performed at beamlines 33 and I311 at the MAX-lab synchrotron-radiation facility in Lund, Sweden. The ARPES spectra were recorded with an angle-resolved photoelectron spectrometer with an angular resolution of ±2°, and the Si 2*p* core-level spectra were obtained with an angle-integrated photoelectron spectrometer with an acceptance angle of ~15°. The total experimental energy resolutions were ~80 meV for the ARPES measurements and ~20 meV for the Si 2*p* measurements. The Si(110) sample, cut from a B-doped (*p*-type, 1–5 Ω cm) Si wafer, was first

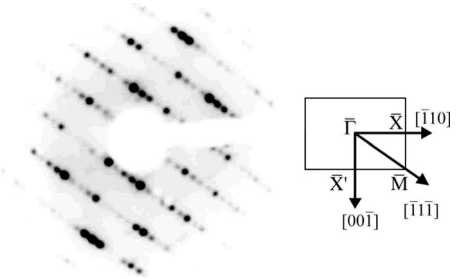

FIG. 1. LEED pattern of the Si(110)-(16×2) surface obtained at 100 K with a primary electron energy of 36 eV and the surface Brillouin zone of the Si(110)-(1×1) surface. 16× spots are clearly observed along the [$\bar{1}1\bar{1}$] direction.

degassed at 900 K for more than 5 h in the vacuum chamber. In order to obtain a clean surface, the sample was annealed at 1520 K for 3 s, quenched to 1200 K within 3 s, cooled down to 1000 K in 1 min, kept at 1000 K for 30 s, and then slowly cooled down to room temperature. After the annealing, a sharp (16×2) low-energy electron diffraction (LEED) pattern was observed and neither the valence-band spectra nor the core-level spectra showed any indication of contamination.

A commercial JEOL JSTM-4500XT system was used for the STM measurements at the National Institute for Materials Science. An electrochemically etched tungsten tip was cleaned *in situ* by electron bombardment and treated on a Pt(111) surface[27] before each measurement to ensure the metallicity of the tip. The LDOS mapping was obtained by a lock-in detection $[(dI/dV)/(I/V)]$ at certain sample biases in a constant current mode.[28] The tunneling current was 0.25 nA, and the modulation frequency and amplitude were 961 Hz and 30 mV, respectively. A small loop gain was selected so that the modulation would not affect the feedback loop. The base pressure was below 4×10^{-11} Torr in both the PES and STM measurements.

III. RESULTS AND DISCUSSION

Taking the twofold symmetry of the Si(110)-(1×1) surface into account, one would expect the presence of a two-domain (16×2) surface. In fact, a two-domain (16×2) surface has been observed using LEED (Refs. 5, 24, and 29) and STM.[16,18,20] Figure 1 shows the LEED pattern of the Si(110)-(16×2) surface obtained at 100 K with a primary electron energy of 36 eV, together with the (1×1) surface Brillouin zone (SBZ). Clear 16× spots are observed along the [$\bar{1}1\bar{1}$] direction only. The absence of 16× spots in the [$\bar{1}$11] direction indicates that, in contrast to the former studies in which a two-domain surface was observed, a very high quality single-domain Si(110)-(16×2) surface was obtained in the present study. This LEED result implies that the ARPES spectra of the Si(110)-(16×2) surface can be analyzed without the ambiguity that would have otherwise been caused by contribution from the other domain. Here we note that the formation of a single-domain (16×2) surface did not depend on the direction of the current sent through the sample for annealing and that a two-domain (16×2) surface was only obtained when the sample was not uniformly heated. This is in contrast to the results reported in Ref. 30, in which the formation of a single-domain surface was reported to depend on the direction of the annealing current.

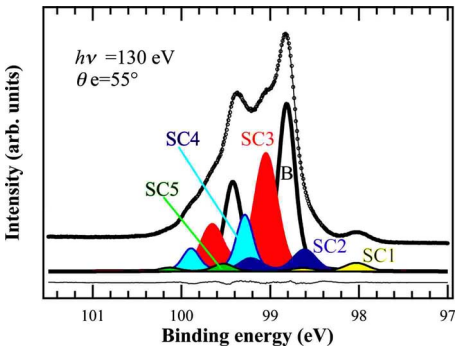

FIG. 2. (Color online) Si 2*p* core-level spectrum of the Si(110)-(16×2) surface measured at $h\nu$=130 eV and θ_e=55°. The open circles are the experimental data and the solid line overlapping the open circles is the result of the fit. Each component is indicated by different shading. The difference between the experimental data and the fit is shown by the lowermost solid line.

In order to confirm the quality of the surface with a higher certainty, we have measured the Si 2*p* core level. Figure 2 shows the Si 2*p* core-level spectrum of the Si(110)-(16×2) surface, measured at 100 K with a photon energy ($h\nu$) of 130 eV and an emission angle (θ_e) of 55°. The Si 2*p* spectrum has been analyzed by a standard least-squares-fitting method using spin-orbit split Voigt functions to obtain information about the components that contribute to the shape of the experimental spectrum (open circles). The solid line overlapping the experimental data is the result of the fit. We used 608 meV for the spin-orbit splitting and a 80 meV full width at half maximum (FWHM) for the Lorentzian contribution for all components in the fitting procedure. The Gaussian width (FWHM) of the bulk component is 190 meV and those of the surface components are between 220 and 260 meV. A polynomial background was subtracted before the decomposition of each spectrum and each component is indicated by different shading. The difference between the experimental data and the fit is indicated at the bottom of the spectrum. From the result of the fitting procedure, we can conclude that the Si(110)-(16×2) surface has six components [one bulk component (B) and five surface components (SC1-SC5)]. The E_B of the surface components relative to that of the bulk component (surface core-level shift, SCLS) are described in Table I. The number of surface components and their SCLSs agree well with those reported in a recent high-resolution photoemission measurement.[26] The narrow Gaussian widths of the surface components that produce the clear observation of features originating from the surface components in the spectrum, the agreement with the former study or the Si 2*p* core-level spectrum, and the sharp LEED pattern prove definitely the high quality of the Si(110)-(16×2) surface used in the present study.

The overall band dispersions of the Si(110)-(16×2) surface along the three symmetry directions of the (1×1) SBZ are shown in Fig. 3. Figures 3(a)–3(c) show the band disper-

TABLE I. SCLSs of the Si 2*p* surface components observed in Fig. 2.

Component	SCLS
SC1	−800 meV
SC2	−290 meV
SC3	250 meV
SC4	470 meV
SC5	710 meV

sions along the $\bar{\Gamma}$-$\bar{X}'$, $\bar{\Gamma}$-$\bar{X}$, and $\bar{\Gamma}$-$\bar{M}$ directions, respectively. The shaded areas are the bulk band projection taken from Ref. 31 and the vertical dashed lines represent the symmetry points of the (1×1) SBZ indicated at the top of each figure. The valence-band maximum (VBM) is estimated from the E_B of the Si 2*p* core level using the relation between $E_{B(\mathrm{VBM})}$, E_F, and $E_{B(\mathrm{Si}\,2p3/2)}$ given in Ref. 32. Two surface states, denoted as S_2 and S_3, are clearly observed in the gap of the bulk band projection in Fig. 3(a), and three surface states (S_2, S_3, and S_4) are observed in the gap in Figs. 3(b) and 3(c). The E_B of these states are S_2: ~0.4 eV, S_3: ~0.75 eV, and S_4: ~1.0 eV. Since the number of surface

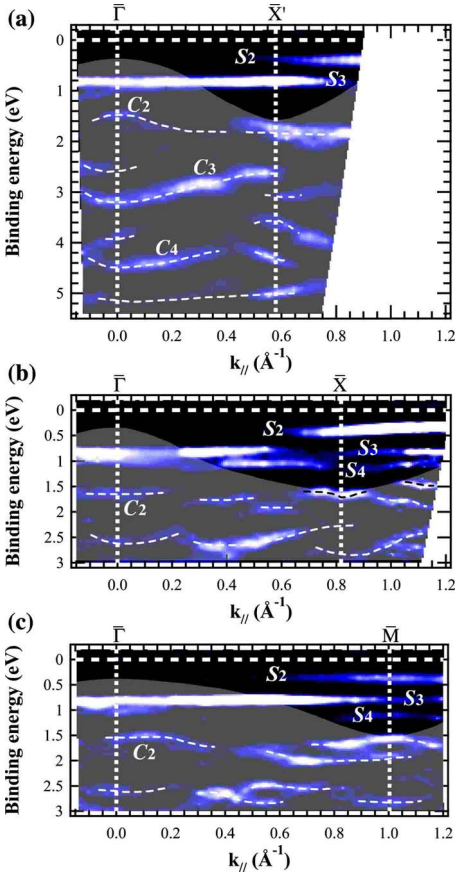

FIG. 3. (Color online) Band dispersions of the Si(110)-(16×2) surface measured along the (a) $\bar{\Gamma}$-$\bar{X}'$, (b) $\bar{\Gamma}$-$\bar{X}$, and (c) $\bar{\Gamma}$-$\bar{M}$ directions using $h\nu$=21.2 eV. The shaded areas are the bulk band projection taken from Ref. 31 and the vertical dashed lines represent the symmetry points indicated at the top of each figure.

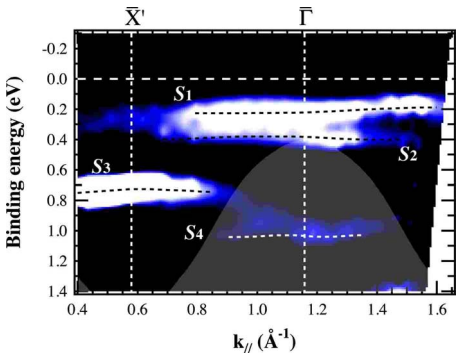

FIG. 4. (Color online) Band dispersions of the Si(110)-(16×2) surface measured from the $\bar{X}'$ point to the $\bar{\Gamma}$ point of the second Brillouin zone along the $[00\bar{1}]$ direction.

states observed along the $\bar{\Gamma}$-$\bar{X}'$ direction is different from those observed along the two other directions, we have measured the ARPES spectra along $\bar{\Gamma}$-$\bar{X}'$-$\bar{\Gamma}$ in more detail to determine the actual number of surface states in the bulk band gap.

Figure 4 shows the band dispersions of the Si(110)-(16×2) surface from the $\bar{X}'$ point to the $\bar{\Gamma}$ point of the second SBZ that are obtained in a high-resolution ARPES measurement. In Fig. 4, a surface state is observed at E_B=1.0 eV together with the S_3 state at E_B=0.75 eV within a E_B range of 0.75–1.0 eV. Taking the almost flat dispersions into account, the E_Bs of the observed states indicate that the S_4 state is present along the $\bar{\Gamma}$-$\bar{X}'$-$\bar{\Gamma}$ direction as well as along the two other directions. Further, the presence of two surface states at E_B less than 0.5 eV is clearly seen in Fig. 4. The E_Bs of these two states are S_1: ~0.2 eV and S_2: ~0.4 eV. Taking these results into account, we conclude that there are four surface states in the bulk band gap. The dispersion widths of the surface states obtained in Fig. 4 are S_1: 30 meV, S_2: 20 meV, S_3: 50 meV, and S_4: 10 meV, values that are much smaller than the widths reported in the former studies (0.5 eV in Ref. 24 and below 0.2 eV in Ref. 26). The very small dispersion widths indicate that although the atomic structure of this surface is one dimensional, the four surface states in the band gap are localized and thus do not show a one-dimensional electronic structure. Moreover, the number of surface states observed in the present study is larger than those reported in the literature (the presence of only one surface state is reported in Ref. 24 and the presence of two states is reported in Ref. 26).

Together with the four surfaces states observed in the band gap, six more states are observed within the projected bulk band at both the $\bar{\Gamma}$ and $\bar{X}'$ points. The E_B of the states are 1.5, 2.6, 3.2, 3.9, 4.5, and 5.15 eV at the $\bar{\Gamma}$ point and 1.8, 2.6, 3.1, 3.6, 4.4, and 5.0 eV at the $\bar{X}'$ point. Of these states, the E_B of the three denoted as C_2, C_3, and C_4 show agreement with those of the "S_2," "S_3," and "S_4" states reported in Ref. 24 and the dispersion behavior of C_4 is similar to that of S_4, i.e., both states show upward dispersions from the $\bar{\Gamma}$ point to the $\bar{X}'$ point. However, the dispersion behaviors of C_2 and C_3 are different from those of S_2 and S_3. The C_2 shows a

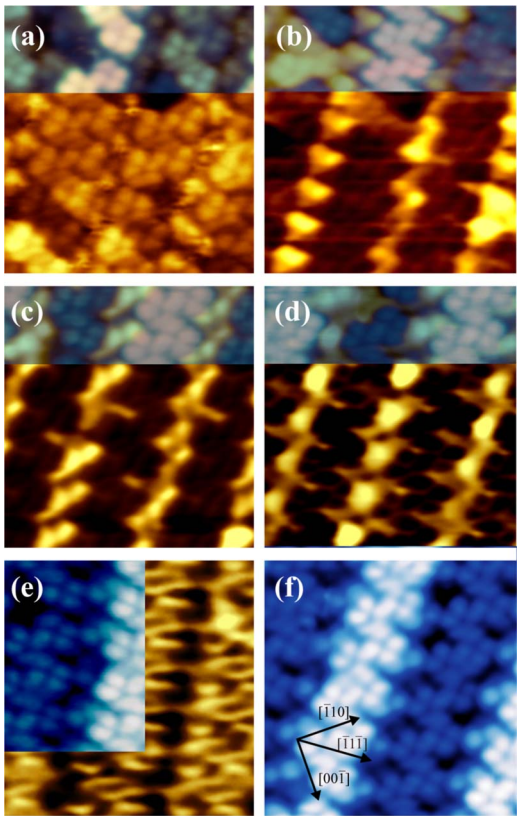

FIG. 5. (Color online) LDOS mappings at E_B=(a) 0.2 eV, (b) 0.4 eV, (c) 0.7 eV, (d) 1.0 eV, and (e) 1.4 eV. The upper parts in (a)–(d) are overlapped with STM images to obtain information about the relation between the LDOS and surface structure. The inset in (e) and (f) are STM images obtained at sample biases of −0.8 and −1.0 V, respectively.

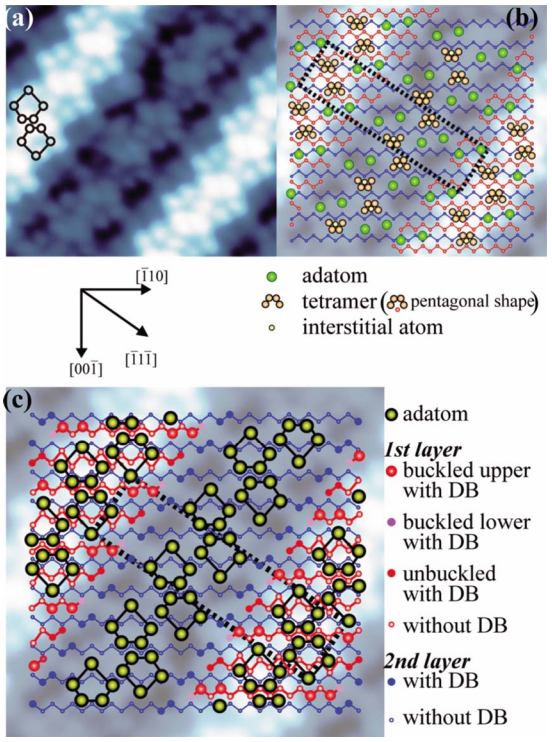

FIG. 6. (Color online) (a) STM image obtained at a sample bias of +0.6 V. A pair of pentamers is indicated at the left side of the figure. (b) ATI model on top of the STM image and (c) the AB model proposed in this paper. The solid lines connecting the adatoms in (a) and (c) are drawn to clarify the pentagonal shape (they do not represent bonds between adatoms).

downward dispersion and C_3 shows an upward dispersion from the $\bar{\Gamma}$ point to the $\bar{X}'$ point, whereas S_2 hardly disperses and S_3 shows a downward dispersion in the corresponding direction. These differences might result from the fact that the photoelectron spectra were recorded at θ_e every 5° in Ref. 24, and thus the dispersion of each state is not represented properly. The E_B of C_2 and C_3 show agreement with those of the "U_1" and "U_2" states reported in Ref. 26 as well. However, although the dispersion behavior of C_2 resembles that of U_1, the dispersion behavior of C_3 is different from that of U_2. Taking into account that there are more than two states in a E_B range of 2–3 eV in Fig. 3, we suppose that the flat dispersion of U_2 is an artifact produced by the presence of several states.

The origins of the surface states observed in the band gap were discussed based on the ATI model in the former study.[26] However, four surface states, two more than the number reported in Ref. 26, are observed in the present study, and thus the origins of the surface states have to be reconsidered. In order to investigate the origins of the states observed in Figs. 3 and 4, we have measured the LDOS mapping at different E_B. Figure 5 shows the LDOS mapping measured at E_B=(a) 0.2 eV, (b) 0.4 eV, (c) 0.7 eV, (d) 1.0 eV, and (e) 1.4 eV, together with an STM image obtained at a sample bias of −1.0 V (a negative sample bias corresponds to the observation of the occupied electronic states). The E_B in Figs. 5(a)–5(d) correspond to those of S_1, S_2, S_3, and S_4, and the E_B in (e) corresponds to that of the C_2 band. As shown in Fig. 5, the LDOS at E_B=0.2 eV is located at the pentamer sites of both the upper terrace and the lower one observed in STM. Regarding the LDOSs at E_B=0.4, 0.7, and 1.0 eV, all of them are located between the neighboring pentamer rows of the upper and lower terraces, but their shapes are different. This means that the origins of the S_2, S_3, and S_4 states are orbitals of Si atoms situated in this area. The LDOSs at E_B=1.4 eV are located slightly off from the pentamer sites.

Figure 6(a) shows an STM image obtained at a sample bias of +0.6 V, and the ATI model is displayed on top of the STM image in Fig. 6(b). By comparing Figs. 6(a) and 6(b), one notices that the pentagonal shape, which is formed by four adatoms and one first layer Si atom in the ATI model, does not fit the pentamer observed in STM, i.e., the pentagonal shape in ATI is much smaller than the pentamer. The adatom sites of the ATI model do not fit the bright sites in the STM image either. These observations imply that the ATI model cannot explain the STM result, and we therefore have to reconsider the atomic structure of Si(110)-(16×2). As one can see from the STM image in Figs. 5(f) and 6(a) and from the STM images reported in the literature, the Si(110)-(16×2) should be composed of surface atoms that form pentamers and an up-and-down regular step arrangement. Further, the similarity between the Si 2p core-level spectra of the Si(110)-(16×2) and Si(111)-(7×7) surfaces

suggests the presence of adatoms on Si(110)-(16×2), and the LDOS in Fig. 5(a) indicates that all the five bright sites forming a pentamer originate from the same surface state S_1.

Of the proposed structural models, the one in Ref. 21 is the only model that contains the up-and-down regular step arrangement and the pentamer whose bright sites are well explained by five adatoms, i.e., by five equivalent surface atoms. However, although this model shows these agreements, it cannot explain the three types of surface states observed between the neighboring pentamers of the upper and lower terraces because there are only two kinds of surface Si atoms, at most, that differ from the bulk Si atoms in this area. By considering the STM result in Ref. 20, in which a first layer Si row with buckled structure is observed, we propose a structural model that consists of adatoms and buckled Si atoms in every second row of the first Si layer [Fig. 6(c)]. (Note that the presence of adatoms lowers the surface energy more than the presence of tetramers and interstitial atoms.[22]) In this adatom-buckling (AB) model, there are four kinds of surface Si atoms with dangling bonds (DBs) between the neighboring pentamers of the upper and lower terraces, that is, the upper and lower Si atoms of the buckled structure, the unbuckled Si atoms of the first layer, and the second layer Si atoms (the outermost atoms of the lower terrace). The atomic structure of this AB model can explain the origins of all the LDOS mappings shown in Fig. 5 and thus those of the four surface states observed in ARPES. That is, the LDOSs at E_B=0.2 and 0.4 eV fit the positions of the adatoms and the upper buckled Si atoms, respectively, the LDOS at E_B=0.7 agrees with the position of the lower buckled Si atoms and the unbuckled first layer Si atoms and that at E_B=1.0 fits the position of the second layer Si atoms. We therefore attribute the origin of S_1 to the DBs of the adatoms, that of S_2 to the DBs of the upper atoms of the buckled Si, S_3 to the DBs of both the lower atoms of buckled Si and the first layer unbuckled Si atoms, and S_4 to the DBs of the second layer Si atoms. Moreover, the LDOS at E_B=1.4 eV suggests that the origin of C_2 would be the back bonds of the adatoms.

The Si $2p$ surface components have only been discussed[26] in terms of the ATI model, which is no longer appropriate, and thus we have to reassign their origins. On a Si(111)-(7×7) surface, the adatoms, the Si atoms bonded to the adatoms, and the rest atoms produce surface components with SCLSs of ~530, ~244, and ~−700 meV, respectively,[33] and the up and down atoms of asymmetric dimers produce surface components with SCLSs of ~−485 and ~62 meV on a Si(001)-c(4×2) surface.[34] The SCLS of the SC3 component observed in Fig. 2 agrees well with that of the Si atoms bonded to the adatoms, and the SCLS of SC4 shows agreement with that of the adatoms of a Si(111)-(7×7) surface. By assuming that the charge states of the adatoms are similar on Si(110) and Si(111) and the charge states of the atoms bonded to adatoms are also similar on the two surfaces, the agreements in SCLSs suggest that the adatoms of the AB model and the unbuckled atoms situated below them contribute to SC4 and SC3, respectively. Regarding the SC1 and SC2 components, their signs are the same as those of the rest atoms and the up atoms of asymmetric dimers. If there is a charge transfer from the adatoms to the DBs of the unbuckled atoms and the second layer atoms with DBs, these atoms and the buckled upper atoms might contribute to SC1 and SC2. The intensity ratio of the five Si $2p$ surface components is SC1: SC2: SC3: SC4: SC5 ~ 1: 3: 16: 6: 1 in Fig. 2, and it was ~2: 5: 30: 10: 1 in the spectrum measured at $h\nu$=130 eV and θ_e=0°. As shown in Table II, the number ratio between the buckled upper, the sum of unbuckled with DB and second layer with DB, the sum of first without DB and second without DB, and the adatom is 4: 12: 46: 20. By considering that this ratio roughly fits the ratio of SC1: SC2: SC3: SC4 and by taking the agreement in SCLS into account, we assign the origin of SC1, SC2, SC3, and SC4 to the buckled upper atoms, the unbuckled atoms and the second layer atoms with DBs, the first and second layers atoms without DBs, and the adatoms, respectively. Concerning the SC5 component, its small intensity suggests that the origin might be the buckled lower atoms.

TABLE II. Number of atoms per unit cell in the AB model. The second layer atoms without DB are the second layer atoms bonded to adatoms (the second layer atoms underneath the first layer ones are excluded).

Layer	Atoms	Number
First	Adatom	20
	Buckled upper	4
	Buckled lower	2
	Unbuckled with DB	4
	Without DB	22
Second	With DB	8
	Without DB	24

IV. CONCLUSION

In conclusion, we have studied the electronic structure of the Si(110)-(16×2) surface along the $\bar{\Gamma}$-$\bar{X}'$, $\bar{\Gamma}$-$\bar{X}$, and $\bar{\Gamma}$-$\bar{M}$ directions of the (1×1) SBZ using ARPES and the LDOS mapping using STM. Four semiconducting surface states, which hardly disperse, were observed in the bulk band gap at E_B=0.2, 0.4, 0.75, and 1.0 eV. Since this number is larger than those reported in the literature, we have reconsidered the origins of the surface states. We have also proposed a structural model that can explain the origins of all the observed surface states on the basis of our experimental results. Taking the E_B of these four states and the LDOS obtained in STM into account, we have assigned the S_1 state to originate from the adatom DBs, S_2 to originate from the DBs of the upper atoms of the buckled Si, the origin of S_3 to the DBs of both the lower buckled Si atoms and the first layer unbuckled Si atoms, and the origin of S_4 to the DBs of the second layer Si atoms. We have also discussed the dispersion behaviors of the six states observed within the projected bulk band and assigned the origin of one of them to the back-bond state of the adatoms. Further, we have reassigned the origins of the surface components observed in the Si $2p$ core-level spectrum based on the AB model proposed in this paper.

ACKNOWLEDGMENTS

Experimental support from T. Balasubramanian and the MAX-laboratory staff and suggestions on the sample preparation from T. An are gratefully acknowledged. This work was financially supported by the Grant-in-Aid for Science Research (A), Contract No. 20244045, from the Ministry of Education, Culture, Sports, Science, and Technology of Japan and the Swedish Research Council.

*kazuyuki_sakamoto@faculty.chiba-u.jp

†Permanent address: Faculty of Mathematics and Physics, Charles University in Prague, Praha 18000, Czech Republic.

[1] Z. He, M. Stevens, D. J. Smith, and P. A. Bennett, Appl. Phys. Lett. **83**, 5292 (2003).

[2] S. Liang, R. Islam, D. J. Smith, P. A. Bennett, J. R. O'Brien, and B. Taylor, Appl. Phys. Lett. **88**, 113111 (2006).

[3] M. Jalochowski and E. Bauer, Surf. Sci. **480**, 109 (2001).

[4] J. L. McChesney, J. N. Crain, F. J. Himpsel, and R. Bennewitz, Phys. Rev. B **72**, 035446 (2005).

[5] T. An, M. Yoshimura, and K. Ueda, Surf. Sci. **576**, 165 (2005).

[6] D. J. Eaglesham, A. E. White, L. C. Feldman, N. Moriya, and D. C. Jacobson, Phys. Rev. Lett. **70**, 1643 (1993).

[7] C.-P. Li, C.-S. Lee, X.-L. Ma, N. Wang, R.-Q. Zhang, and S.-T. Lee, Adv. Mater. **15**, 607 (2003).

[8] R.-Q. Zhang, Y. Lifshitz, and S.-T. Lee, Adv. Mater. **15**, 635 (2003).

[9] J. D. Holmes, K. P. Johnston, R. C. Doty, and B. A. Korgel, Science **287**, 1471 (2000).

[10] D. D. D. Ma, C. S. Lee, F. C. K. Au, S. Y. Tong, and S. T. Lee, Science **299**, 1874 (2003).

[11] T.-L. Chan, C. V. Ciobanu, F.-C. Chuang, N. Lu, C.-Z. Wang, and W.-M. Ho, Nano Lett. **6**, 277 (2006).

[12] S. Sugawa, I. Ohshima, H. Ishino, Y. Saito, M. Hirayama, and T. Ohmi, Tech. Dig.-Int. Electron Devices Meet. (2001), p. 37.3.1-4.

[13] K. Arima, J. Katoh, S. Horie, K. Endo, T. Ono, S. Sugawa, H. Akahori, A. Teramoto, and T. Ohmi, J. Appl. Phys. **98**, 103525 (2005).

[14] H. Ampo, S. Miura, K. Kato, Y. Ohkawa, and A. Tamura, Phys. Rev. B **34**, 2329 (1986).

[15] Y. Yamamoto, S. Ino, and T. Ichikawa, Jpn. J. Appl. Phys., Part 2 **25**, L331 (1986).

[16] E. J. van Loenen, D. Dijkkamp, and A. J. Hoeven, J. Microsc. **152**, 487 (1988).

[17] Y. Yamamoto, Phys. Rev. B **50**, 8534 (1994).

[18] W. E. Packard and J. D. Dow, Phys. Rev. B **55**, 15643 (1997).

[19] Y. Yamamoto, T. Sueyoshi, T. Sato, and M. Iwatsuki, Surf. Sci. **466**, 183 (2000).

[20] T. An, M. Yoshimura, I. Ono, and K. Ueda, Phys. Rev. B **61**, 3006 (2000).

[21] T. Ichikawa, Surf. Sci. **544**, 58 (2003).

[22] A. A. Stekolnikov, J. Furthmüller, and F. Bechstedt, Phys. Rev. Lett. **93**, 136104 (2004).

[23] A. A. Stekolnikov, J. Furthmüller, and F. Bechstedt, Phys. Rev. B **70**, 045305 (2004).

[24] A. Cricenti, B. Nesterenko, P. Perfetti, G. LeLay, and C. Sebenne, J. Vac. Sci. Technol. A **14**, 2448 (1996).

[25] L. Grill, A. Santoni, S. Prato, L. Petaccia, and S. Modesti, Surf. Sci. **474**, 55 (2001).

[26] N. D. Kim, Y. K. Kim, C.-Y. Park, H. W. Yeom, H. Koh, E. Rotenberg, and J. R. Ahn, Phys. Rev. B **75**, 125309 (2007).

[27] J. Mysliveček, A. Stróżecka, J. Steffl, P. Sobotík, I. Ošt'ádal, and B. Voigtländer, Phys. Rev. B **73**, 161302(R) (2006).

[28] R. M. Feenstra, J. A. Stroscio, and A. P. Fein, Surf. Sci. **181**, 295 (1987).

[29] Y. Sakamoto, Y. Fukui, J. Takeuchi, S. Hongo, and T. Urano, Surf. Rev. Lett. **10**, 467 (2003).

[30] Y. Yamada, A. Girard, H. Asaoka, H. Yamamoto, and S. I. Shamoto, Phys. Rev. B **76**, 153309 (2007); **77**, 153305 (2008).

[31] I. Ivanov, A. Mazur, and J. Pollmann, Surf. Sci. **92**, 365 (1980).

[32] F. J. Himpsel, G. Hollinger, and R. A. Pollak, Phys. Rev. B **28**, 7014 (1983).

[33] C. J. Karlsson, E. Landemark, Y.-C. Chao, and R. I. G. Uhrberg, Phys. Rev. B **50**, 5767(R) (1994).

[34] E. Landemark, C. J. Karlsson, Y.-C. Chao, and R. I. G. Uhrberg, Phys. Rev. Lett. **69**, 1588 (1992).